UNIVERSITÉ LAVAL

On-chip Fourier transform spectrometers by dual-polarized detection

Huijie Wang, Zhongjin Lin, Qifeng Li, and Wei Shi

OSA Optics Letters, (Volume 44, Issue 11) (2019)

Doi: 10.1364/OL.44.002923

https://doi.org/10.1364/OL.44.002923

© 2019 Optical Society of America. One print or electronic copy may be made for personal use only. Systematic reproduction and distribution, duplication of any material in this paper for a fee or for commercial purposes, or modifications of the content of this paper are prohibited.

Copyright (c) 2019 OSA. Personal use is permitted. For any other purposes, permission must be obtained from the Optical Society of America by emailing copyright@osa.org.

On-chip Fourier transform spectrometers by dual-polarized detection

Huijie Wang,[1,2] Zhongjin Lin,[1] Qifeng Li,[2,3] and Wei Shi[1,4]

[1]*Department of Electrical and Computer Engineering, Center for Optics, Photonics and Lasers (COPL), Université Laval, Québec, QC G1V 0A6, Canada*
[2]*School of Precision Instrument and Opto-electronics Engineering, Tianjin University, Tianjin 300072, China*
[3]*e-mail: qfli@tju.edu.cn*
[4]*e-mail: wei.shi@gel.ulaval.ca*

Chip-scale Fourier transform spectrometers (FTSs) have recently emerged for inexpensive, high-resolution spectroscopic applications. In particular, spatial-heterodyne FTSs (SH-FTSs) have drawn considerable attention with a simple and stable configuration based on an array of Mach–Zehnder interferometers (MZIs) with linearly increased optical path differences. There is a significant trade-off between spectral performance and the MZI number. In this work, we propose a dual-polarized SH-FTS, detecting both fundamental transverse electric and transverse magnetic modes, on a silicon photonic chip. Our experimental results show that, compared to the conventional single-polarized design, the MZI number of the dual-polarized SH-FTS can be nearly halved for a smaller footprint with little compromise of spectral performance.

Fourier transform spectrometers (FTSs) have been widely applied for high-resolution spectral measurements in various fields, including chemical detection, environmental monitoring, and astronomical exploration, especially in weak-signal applications with inherent multiplex advantage [1–4]. The spectral resolution of FTSs is fundamentally determined by the maximum optical path difference (OPD) generated during the interference measurement, which has no limit to the optical throughput [5]. Thoroughly different from the multiplexing FTSs, the dispersive counterparts commonly measure the light of different wavelengths separately in the temporal or spatial domain, which leads to the considerable reduction in the optical throughput captured by a single detector. Consequently, there will be an obvious deterioration of the signal-to-noise ratio (SNR), when the detector noise is dominant [5,6]. Since the higher resolution is inevitably accompanied by the lower throughput, a significant trade-off exists between the spectral resolution and SNR for dispersive spectrometers. In this sense, FTSs are more suitable for on-chip low-power measurements than dispersive spectrometers, benefiting from a higher SNR.

Chip-scale FTSs have achieved significant progress by means of photonic integrated circuits (PICs) in recent years, with the proven performance of high resolution and high throughput [7]. Active scanning FTSs (AS-FTSs) produce the linearly increasing OPDs by either thermo-optically or electro-optically tuning the refractive index of optical waveguides [8,9] or adjusting the optical path lengths through cascaded sets of thermo-optic switches [10,11]. While AS-FTSs based on a single-interferometer configuration have a higher throughput, the strong influence of the instability in the tuning control is of great concern. Stationary-wave-integrated FTSs (SWI-FTSs) capture the interference of the evanescent fields of two copropagating waveguide modes by single-shot imaging [12,13], which are based on a stable but much more complicated structure. Spatial-heterodyne FTSs (SH-FTSs) with a simpler and more stable architecture are implemented based on an array of Mach–Zehnder interferometers (MZIs) with uniform-spacing OPDs [14–17]. The interferogram is usually captured spatially by a linear detector array.

Nevertheless, the spectral resolution and bandwidth of SH-FTSs are closely related with the number of sampling MZIs, which always requires a balance to meet the limited chip scale and detecting conditions. To break through this restriction, the compressive-sensing technique has been introduced to reduce the sampling MZI number to one-fourth by numerical processing; however, the input spectra have to be sparse [18,19]. The exiting SH-FTSs are always based on the detection of one certain waveguide mode, i.e., the fundamental transverse electric (TE) or transverse magnetic (TM) mode. As the two polarized modes have different propagation constants, it is promising to acquire sufficient interference information for achieving equal spectral performance with fewer MZIs through the detection of both TE and TM modes.

In this Letter, we propose a dual-polarized SH-FTS applying both the fundamental TE and TM modes, demonstrating that the number of sampling MZIs can be nearly halved, while the spectral performance is well maintained with a resolution of 27.5 pm and a bandwidth of 440 pm. First, the configuration of the proposed dual-polarized SH-FTS is introduced, in which the waveguide widths are adapted for realizing a uniform-spacing OPD sequence according to the propagation constants

National Science and Engineering Research Council of Canada (NSERC) Funding: STPGP 494358-16

Copyright (c) 2019 OSA. Personal use is permitted. For any other purposes, permission must be obtained from the Optical Society of America by emailing copyright@osa.org.

of TE and TM modes. Then we present our numerical design and experimental results. A calibration matrix of the implemented dual-polarized SH-FTS is acquired through the high-resolution wavelength-scanning measurement, in order to retrieve the input spectra using its pseudoinverse. Finally, for the purpose of demonstration, laser spectra with different wavelength distributions are extracted using the Penrose–Moore pseudoinverse method, whose spectral performance agrees well with the reference spectra measured by a traditional TE-polarized SH-FTS fabricated on the same chip.

As schematically shown in Fig. 1, our proposed dual-polarized SH-FTS is composed of an array of MZIs with different waveguide widths and arm imbalances. Different from conventional single-polarized SH-FTSs [14], our device is designed to accept both TE and TM modes for dual-polarized detection. The single-polarized SH-FTSs are composed of waveguides with an identical width, where each MZI contributes one specific OPD value. In our proposed structure, each MZI contributes two OPD values, one from the TE mode and the other from the TM mode, except for the first MZI in a balanced design (OPD = 0); the waveguide width is varied as the OPD order to build up a sequence of linearly increasing OPDs, $0, \alpha_1 n_{\mathrm{TE}1}\Delta L_1, n_{\mathrm{TE}1}\Delta L_1, \ldots, \alpha_i n_{\mathrm{TE}i}\Delta L_i, n_{\mathrm{TE}i}\Delta L_i, \ldots,$ according to

$$\alpha_{i+1} = \frac{\alpha_i - 2}{2\alpha_i - 3} \quad (\alpha_1 = 0.5), \tag{1}$$

$$\Delta L_{i+1} = \frac{1 - \alpha_i}{1 - \alpha_{i+1}} \Delta L_i, \tag{2}$$

where $n_{\mathrm{TE}i}$ is the effective index of TE mode, α_i is the effective index ratio of TM to TE mode ($n_{\mathrm{TM}}/n_{\mathrm{TE}}$) and ΔL_i is the arm imbalance in the i-th MZI. Following the Rayleigh criterion [11], the wavelength resolution $\delta\lambda$ and bandwidth $\Delta\lambda$ of an SH-FTS are determined by the maximum arm imbalance $\Delta L_{\max}$ and the imbalanced MZI number N according to

$$\delta\lambda = \frac{\lambda_0^2}{\Delta L_{\max} n_g}, \tag{3}$$

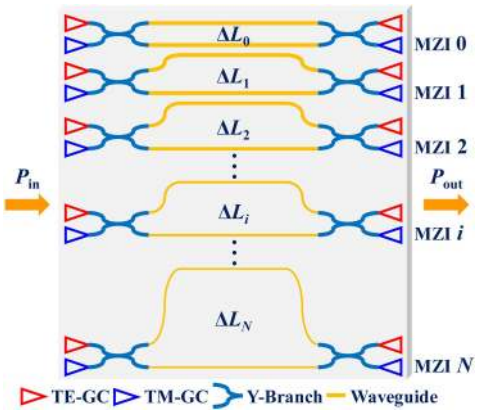

Fig. 1. Schematic diagram of the proposed dual-polarized SH-FTS consisting of a group of MZIs with different waveguide widths and arm imbalances. For emphasizing the dual-polarized detection scheme, TE- and TM-mode grating couplers are used for the inputs and outputs of light.

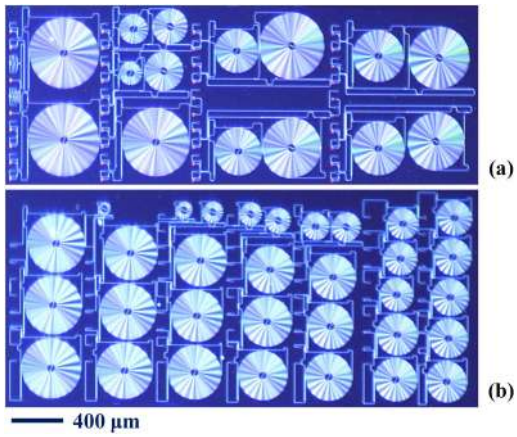

Fig. 2. Optical micrographs of the fabricated SH-FTSs using the electron beam lithography technique: (a) dual-polarized SH-FTS composed of 17 imbalanced MZIs; (b) TE-polarized SH-FTS composed of 32 imbalanced MZIs, as a reference. TE- and TM-mode grating couplers were used as the input and output ports of light.

$$\Delta\lambda = \delta\lambda \frac{N}{2}, \tag{4}$$

where λ_0 is the central wavelength and n_g is the group index of the waveguide of $\Delta L_{\max}$ (ΔL_N in Fig. 1).

As each MZI is measured twice in orthogonal polarizations, the total required number of MZIs can be approximately halved for the same spectral resolution. Polarization-selective grating couplers with Y-branches are used as optical input and output ports for test simplicity, as shown in Fig. 1. They can be replaced by edge couplers and broadband couplers to reduce insertion loss and thus increase throughput.

As a demonstration, a dual-polarized SH-FTS composed of 17 imbalanced MZIs was fabricated on a silicon-on-insulator wafer with a 220-nm-thick silicon waveguide layer and a 2-μm-thick buried oxide (BOX) layer using the electron beam lithography. A photograph of the fabricated device is shown in Fig. 2(a). In this device, a uniform-spacing OPD sequence was designed for up to 4.805 cm in a 0.150 cm step, achieving a spectral resolution of 27 pm and a bandwidth of 432 pm around the central wavelength of 1550 nm following Eqs. (3) and (4). The waveguide widths and arm imbalances were chosen according to Eqs. (1) and (2). Figure 3 shows the

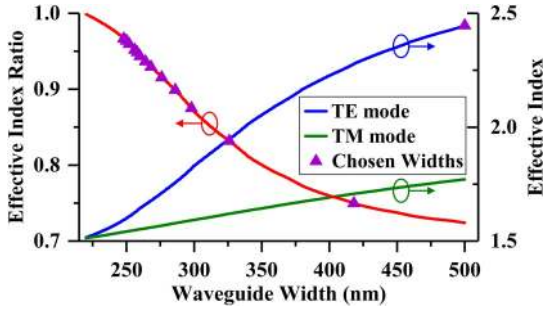

Fig. 3. Effective indexes of the TE and TM modes and their ratio (TM to TE, i.e., α) varying with the waveguide width. The minimum effective index ratio cannot reach 0.5, requiring the replacement by two TE-polarized MZIs with 500 nm wide waveguides. The chosen waveguide widths are marked.

National Science and Engineering Research Council of Canada (NSERC) Funding: STPGP 494358-16

Copyright (c) 2019 OSA. Personal use is permitted. For any other purposes, permission must be obtained from the Optical Society of America by emailing copyright@osa.org.

effective indexes of both TE and TM modes and their ratio (α) varying with the waveguide width. Since the minimum effective index ratio cannot reach 0.5, two TE-polarized MZIs with a waveguide width of 500 nm were used to replace the first unbalanced MZI (ΔL_1 in Fig. 1, corresponding to the minimum arm imbalance). As marked in Fig. 3, the maximum waveguide width is 500 nm, corresponding to the minimum arm imbalance of 0.061 cm. The minimum waveguide width was chosen to be 248 nm, corresponding to the maximum arm imbalance of 3.026 cm. For a reference, a traditional TE-polarized SH-FTS with an approximately equal spectral performance was fabricated on the same wafer, as shown in Fig. 2(b). The TE-polarized SH-FTS consists of 32 imbalanced MZIs with a single waveguide width of 500 nm, whose footprint is about 1.33 times that of the dual-polarized SH-FTS.

The pseudoinverse method has been recognized as a more effective spectral reconstruction method for on-chip SH-FTSs than the conventional Fourier transform method, as the OPD errors resulting from the inevitable fabrication variability can be compensated through numerical processing more conveniently than physical tuning [14,15]. In the spectral reconstruction process, the calibration matrix A of the SH-FTS is needed to retrieve the input spectrum S from the output interferogram I using its pseudoinverse A^+, according to the linear relationship $AS = I$ and $A^+I = S$. In the calibration matrix, the rows correspond to different OPD indexes, and the columns correspond to various wavelengths. For acquiring the calibration matrix, a high-resolution tunable laser (Agilent 81640B) was used as the input source. The wavelength was scanned in a 2.5 pm step over a 500 pm spectral range with an output power of −5 dBm covering the full bandwidth. A polarization controller was used to switch the input polarization state for exciting the TE or TM mode. Figure 4 shows the calibration matrix of the dual-polarized SH-FTS in the wavelength range from 1549.73 nm to 1550.17 nm, with distinct interference fringes varying with the laser wavelength and regular free spectral ranges (FSRs) varying with the imbalanced MZIs. The interference fringes detected in the TE mode (marked in red) have obviously poorer visibility than the TM mode (marked in blue), which is primarily due to the larger propagation loss.

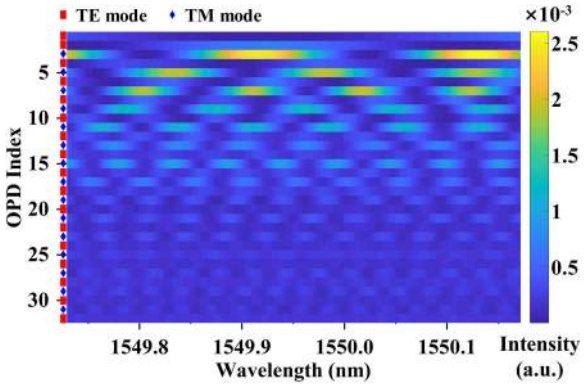

Fig. 4. Calibration matrix of the dual-polarized SH-FTS acquired by the high-resolution wavelength-scanning measurement, showing distinct interference fringes varying with the laser wavelengths and regular FSRs varying with the imbalanced MZIs. TE-mode detection is marked in red, and TM-mode detection is marked in blue.

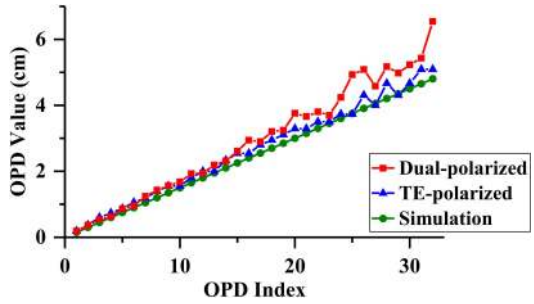

Fig. 5. Simulated and experimentally extracted OPD values of the fabricated dual-polarized SH-FTS and TE-polarized SH-FTS (as a reference) calculated from the FSRs.

The measured OPDs in the dual-polarized SH-FTS and TE-polarized SH-FTS were calculated using the measured FSRs, as shown in Fig. 5. The OPDs in the dual-polarized SH-FTS show a bigger fluctuation, with the OPD error of 0.5981 cm by the root mean square (rms) value, while the TE-polarized SH-FTS has a smaller OPD error of 0.2137 cm. The imperfect OPD sequence has a negative influence on the spectral extraction.

Figure 6 shows the normalized spectra of two laser lines with varied wavelength spacing measured by the dual-polarized SH-FTS and TE-polarized SH-FTS, using the Penrose–Moore pseudoinverse method. A Gaussian apodization window was applied to suppress the truncation ripples by convolution [6]. The corresponding simulated spectra are also plotted together to show the accuracy of spectral extraction. The peaks in the

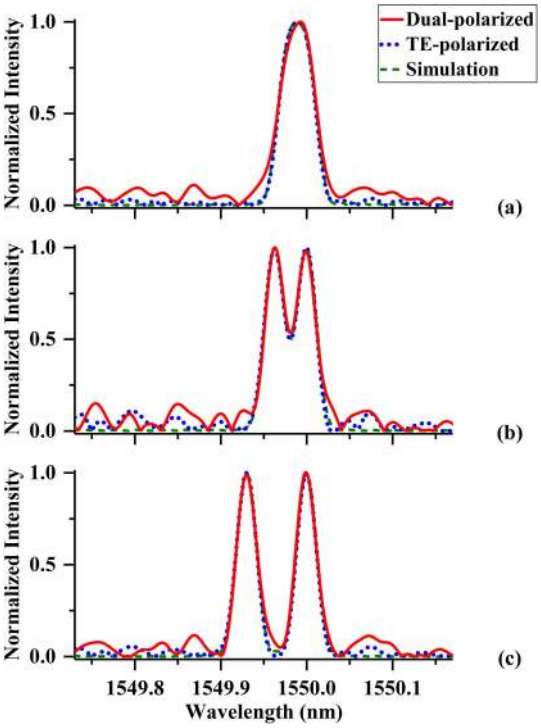

Fig. 6. Simulated and measured spectra of two laser lines by the dual-polarized SH-FTS and TE-polarized SH-FTS (as a reference) with a spacing of (a) 22.5 pm, (b) 37.5 pm, and (c) 70.0 pm.

National Science and Engineering Research Council of Canada (NSERC) Funding: STPGP 494358-16

Copyright (c) 2019 OSA. Personal use is permitted. For any other purposes, permission must be obtained from the Optical Society of America by emailing copyright@osa.org.

two extracted spectra agree well with the simulation for all the cases, showing comparable spectral performance between the dual-polarized SH-FTS and TE-polarized SH-FTS. This excellent agreement also proves the effectiveness of spectral extraction through the pseudoinverse calculation. For the laser line spacing of 22.5 pm, only one peak is observed. As the laser line spacing increases to 37.5 pm, two peaks can be distinguished. The two peaks are completely resolved when the laser line spacing is increased to 70.0 pm. The spectral resolution is 27.5 pm in terms of full width at half-maximum (FWHM), corresponding to a bandwidth of 440 pm.

In addition to the further miniaturized footprint, the dual-polarized SH-FTSs with nearly half sampling MZIs can improve the performance of spectral detection with some specific input designs, benefiting from the significantly fewer input ports supporting both TE and TM modes. For the common single-aperture input scheme that splits light equally into different MZI [14,16], the optical throughput entering every MZI can be increased by about 3 dB for a better SNR. For the enhanced single-aperture input scheme where the input is switched sequentially to each of the MZIs for an even higher throughput [7], the ports of switches can also be reduced by nearly half for faster measurement. For the multiaperture input scheme that provides every MZI with an independent input aperture [15], the influence of nonuniform illumination can be reduced with a smaller incident spot when polarization-independent optical inputs are used.

In summary, a silicon photonic dual-polarized SH-FTS is proposed, for the first time, using both fundamental TE and TM modes. The extracted spectra have been compared with those acquired by the traditional single-polarized SH-FTS, showing that the sampling MZI number can be reduced by nearly half, leading to a smaller footprint without sacrificing the spectral performance. The dual-polarized detection has great potential in further optimizing the on-chip SH-FTS systems for various practical sensing applications.

Funding. Natural Sciences and Engineering Research Council of Canada (NSERC) (STPGP 494358-16); China Scholarship Council (CSC) (201706250049).

Acknowledgment. Huijie Wang thanks the China Scholarship Council (CSC).

REFERENCES

1. D. A. Burns and E. W. Ciurczak, *Handbook of Near-Infrared Analysis* (CRC Press, 2007).
2. N. P. Vidal, E. Goicoechea, M. J. Manzanos, and M. D. Guillén, J. Sci. Food Agric. **94**, 1340 (2014).
3. H. Wang, X. Ma, Y. Wang, D. Chen, W. Chen, and Q. Li, Opt. Express **25**, 19077 (2017).
4. G. Xue, Prog. Polym. Sci. **22**, 313 (1997).
5. V. Saptari, *Fourier-Transform Spectroscopy Instrumentation Engineering* (SPIE, 2003).
6. P. R. Griffiths and J. A. De Haseth, *Fourier Transform Infrared Spectrometry* (Wiley, 2007).
7. B. I. Akca, Opt. Express **25**, 1487 (2017).
8. M. C. Souza, A. Grieco, N. C. Frateschi, and Y. Fainman, Nat. Commun. **9**, 665 (2018).
9. J. Li, D. Lu, and Z. Qi, Opt. Lett. **39**, 3923 (2014).
10. R. A. Soref, F. D. Leonardis, V. M. N. Passaro, and Y. Fainman, J. Lightwave Technol. **36**, 5160 (2018).
11. D. M. Kita, B. Miranda, D. Favela, D. Bono, J. Michon, H. Lin, T. Gu, and J. Hu, Nat. Commun. **9**, 4405 (2018).
12. X. Nie, E. Ryckeboer, G. Roelkens, and R. Baets, Opt. Express **25**, A409 (2017).
13. E. Le Coarer, S. Blaize, P. Benech, I. Stefanon, A. Morand, G. Lérondel, G. Leblond, P. Kern, J. M. Fedeli, and P. Royer, Nat. Photonics **1**, 473 (2007).
14. A. V. Velasco, P. Cheben, P. J. Bock, A. Delâge, J. H. Schmid, J. Lapointe, S. Janz, M. L. Calvo, D.-X. Xu, M. Florjańczyk, and M. Vachon, Opt. Lett. **38**, 706 (2013).
15. H. Podmore, A. Scott, P. Cheben, C. Sioris, P. Cameron, J. H. Schmid, A. Lohmann, Z. Corriveau, and R. Lee, Opt. Express **25**, 33018 (2017).
16. A. Herrero-Bermello, A. V. Velasco, H. Podmore, P. Cheben, J. H. Schmid, S. Janz, M. L. Calvo, D.-X. Xu, A. Scott, and P. Corredera, Opt. Lett. **42**, 2239 (2017).
17. Q. Liu, J. M. Ramirez, V. Vakarin, X. L. Roux, C. Alonso-Ramos, J. Frigerio, A. Ballabio, E. T. Simola, D. Bouville, L. Vivien, G. Isella, and D. Marris-Morini, Opt. Lett. **43**, 5021 (2018).
18. H. Podmore, A. Scott, P. Cheben, A. V. Velasco, J. H. Schmid, M. Vachon, and R. Lee, Opt. Lett. **42**, 1440 (2017).
19. H. Podmore, A. Scott, and R. Lee, IEEE Photon. J. **10**, 6602010 (2018).

202.113.176.159 {ts '2019-06-02 11:25:32'}